

# Capture cross sections on unstable nuclei

A.P. Tonchev<sup>1,a</sup>, J.E. Escher<sup>1</sup>, N. Scielzo<sup>1</sup>, P. Bedrossian<sup>1</sup>, R.S. Ilieva<sup>2,3</sup>, P. Humby<sup>2,3</sup>, N. Cooper<sup>3</sup>, P.M. Goddard<sup>2</sup>, V. Werner<sup>3,6</sup>, W. Tornow<sup>4,5</sup>, G. Rusev<sup>7</sup>, J.H. Kelley<sup>8</sup>, N. Pietralla<sup>6</sup>, M. Scheck<sup>6</sup>, D. Savran<sup>10</sup>, B. Löher<sup>10</sup>, S.W. Yates<sup>9</sup>, B.P. Crider<sup>9</sup>, E.E. Peters<sup>9</sup>, and N. Tsoneva<sup>11</sup>, and S. Goriely<sup>12</sup>

<sup>1</sup> Lawrence Livermore National Laboratory, Livermore, CA 94550, USA

<sup>2</sup> Department of Physics, University of Surrey, Guildford GU2 7XH, UK

<sup>3</sup> Wright Nuclear Structure Laboratory, Yale University, New Haven, Connecticut 06520, USA

<sup>4</sup> Department of Physics, Duke University, Durham, North Carolina 27708, USA

<sup>5</sup> Triangle Universities Nuclear Laboratory, Durham, North Carolina 27708, USA

<sup>6</sup> Institut für Kernphysik, TU Darmstadt, Schlossgartenstrasse 9, 64289 Darmstadt, Germany

<sup>7</sup> Los Alamos National Laboratory, Los Alamos, New Mexico 87545, USA

<sup>8</sup> North Carolina State University, Raleigh, North Carolina 27695, USA

<sup>9</sup> Department of Physics & Astronomy, University of Kentucky, Lexington, Kentucky 40506, USA

<sup>10</sup> ExtreMe Matter Institute and Research Division, GSI, Plankstraße 1, 64291 Darmstadt, Germany

<sup>11</sup> Universität Gießen, Heinrich-Buff-Ring 16, 35392 Gießen, Germany

<sup>12</sup> Institut d'Astronomie et d'Astrophysique, Université Libre de Bruxelles, CP. 226, 1050 Brussels, Belgium

**Abstract.** Accurate neutron-capture cross sections on unstable nuclei near the line of beta stability are crucial for understanding the *s*-process nucleosynthesis. However, neutron-capture cross sections for short-lived radionuclides are difficult to measure due to the fact that the measurements require both highly radioactive samples and intense neutron sources. Essential ingredients for describing the  $\gamma$  decays following neutron capture are the  $\gamma$ -ray strength function and level densities. We will compare different indirect approaches for obtaining the most relevant observables that can constrain Hauser-Feshbach statistical-model calculations of capture cross sections. Specifically, we will consider photon scattering using monoenergetic and 100% linearly polarized photon beams. Challenges that exist on the path to obtaining neutron-capture cross sections for reactions on isotopes near and far from stability will be discussed.

## 1. Introduction

Neutron capture has been studied for decades due to the important ramifications on basic and applied fields such as astrophysics and nuclear energy. In astrophysics, neutron capture reactions span a tremendous range of nuclei needed to account for the creation of elements heavier than iron. Dipole photoabsorption cross sections are important prerequisites for calculations of radiative processes in nuclei where the neutron capture has a major contribution to the nucleosynthesis of heavier elements. Nuclear energy programs depend in part on our ability to understand the reaction rates on stable and radioactive nuclei. Reactions of interest often concern unstable or even exotic (neutron-rich, neutron-deficient, super-heavy) nuclei for which no experimental data exist. At present, direct experimental access to neutron capture on unstable (radioactive) nuclei is limited, and theoretical calculations of these cross sections are comparatively unreliable - uncertainties are often on the order of 100% or even higher. In this paper we try to identify the most relevant observables for constraining the capture cross section on unstable and near the  $\beta$ -stability line nuclei.

## 2. Theoretical formalism

The current state-of-the-art tools for calculating neutron capture cross sections are based on using the Hauser-Feshbach (HF) statistical formalism [1] with input parameters such as nuclear level densities,  $\gamma$ -ray strength functions ( $\gamma$ SF) coming from systematics, and the nucleon-nucleus optical model potential. Within the HF statistical reaction model, the cross section for radiative neutron capture is formulated in terms of the neutron and  $\gamma$  transmission coefficients  $T_n$  and  $T_\gamma$ .

$$\sigma_{n\gamma} = \frac{\pi}{k_n^2} \sum_{j,\pi} g_J \frac{T_\gamma(E, J, \pi) T_n(E, J, \pi)}{T_{\text{tot}}} \quad (1)$$

where  $k_n$  is the incident neutron wave number;  $E$ ,  $J$ , and  $\pi$  are the energy, spin, and parity of a compound state;  $g_J$  is the statistical factor;  $T_{\text{tot}} = T_\gamma + T_n$ .

$T_\gamma$  is given by:

$$T_\gamma(E, J, \pi) = \sum_{X\lambda} \int T_{X\lambda}(E_\gamma) \rho(E - E_\gamma) dE_\gamma \quad (2)$$

Thus,  $T_\gamma(E)$  includes an integration of the product of the partial coefficient  $T_{X\lambda}^m(E_\gamma)$  and the nuclear level density  $\rho(E_m)$  over the energy  $E_m$  of the mediating states, where

<sup>a</sup> e-mail: tonchev2@llnl.gov

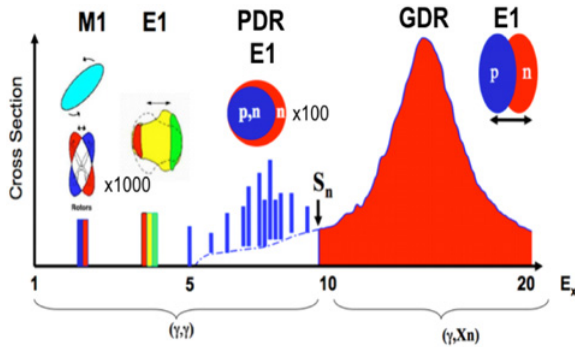


**Figure 1.** Isovector E1 GDR perceived as an oscillation of neutrons against protons. At excitation energies below the neutron separation ( $S_n$ ), a PDR coexists with the tail of the GDR and other dipole excitations such as the orbital M1 scissor mode, spin-flip giant M1 resonance and the E1 and M1 two-phonon excitations.

$E_\gamma = E - E_m$ . When applied to radiative captures, the total photon transmission coefficient entering the calculation of the capture cross section is dominated by E1 transitions. The partial  $\gamma$  transmission coefficient  $T_{x\lambda}(E_\gamma)$  is related to the downward  $\gamma$ -ray strength function  $f(E_\gamma) \downarrow$  by  $T_\gamma^m(E_\gamma) = 2\pi E_\gamma^3 f(E_\gamma) \downarrow$ . The  $f(E_\gamma) \downarrow$  can be measured by photo-disintegration on the basis of the Brink hypothesis, which includes an assumption of the equality between  $f(E_\gamma) \downarrow$  and  $f(E_\gamma) \uparrow$ . The  $f(E_\gamma) \uparrow$  is related to the photoabsorption cross section by  $\sigma_{\text{abs}}(E_\gamma) = 3(\pi hc)^2 E_\gamma f(E_\gamma) \uparrow$ , which in turn can be derived from the photoneutron cross section by  $\sigma_{\gamma,n} = \sigma_{\text{abs}} T_n / (T_n + T_\gamma)$ .

The calculation of the E1-strength function necessitates the knowledge of the low-energy tail of the GDR, governed by the  $(\gamma, \gamma')$  cross section below the neutron separation energy [2]. Figure 1 shows the main modes of excitations which take place below the GDR. As can be seen, the Pygmy Dipole Resonance (PDR) defines a specific relief of the nuclear dipole response at the tail of the GDR. Measurements at the High Intensity Gamma-Ray Source (HI $\gamma$ S) facility using monoenergetic and 100% polarized photon beams confirmed the theoretical predictions that the PDR is dominated by E1 excitations [3,4]. Recent experimental and advanced microscopic theoretical studies of the low-energy dipole response of N = 82 and N = 50 isotopes indicate the existence of M1 dipole strength below and closely above the neutron threshold which is related to the excitation of the isovector spin-flip giant resonance [4,5]. However, the determination of neutron-capture reaction rates is based on ‘pure’ statistical HF codes which do not account for M1 contributions. Furthermore, higher-order multipole admixtures e.g., E2 strengths, should be also included to the total photon-transmission coefficient, even though they are expected to have a minuscule amount of the total  $\gamma$ SF.

### 3. Experimental techniques

For this analysis we illustrate how the Nuclear Resonance Fluorescence (NRF) technique [4–8] can be used to obtain the capture cross section on  $^{75}\text{Ge}$ . Our capture cross-section results will be compared to the recently obtained capture cross-section data on the same  $^{75}\text{Ge}$  branching-point nucleus using  $\beta$ -delayed  $\gamma$  and neutron spectra

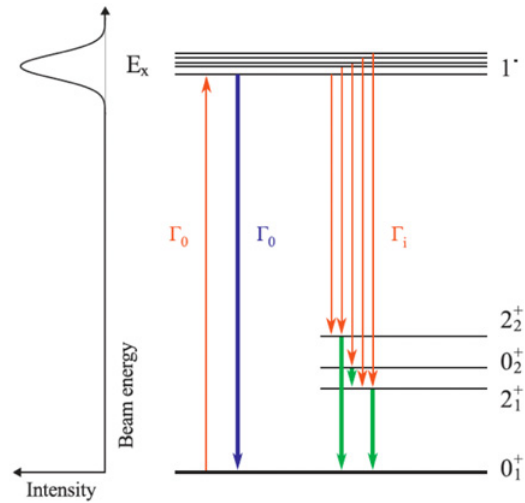


**Figure 2.** The NRF measurements at the HI $\gamma$ S facility. The photon beam distribution from a single incident energy is shown on the left side of a generic decay scheme. The monoenergetic beam excites only levels under energy spread of the beam. Levels decaying to the ground state and from the low-lying excited states ( $2+$ ,  $0+$ , ect.) to the ground state are also measured.

[10, 11]. More detailed information on the advantages and challenges of calculating the capture cross section using indirect techniques, including the surrogate method [12], can be found in Refs. [9, 13].

The technique used for these studies is nuclear resonance fluorescence (NRF) shown in Fig. 2. The nuclear dipole response of  $^{76}\text{Ge}$  in the energy range from 4 to 9 MeV has been measured using a  $(\gamma, \gamma')$  polarized scattering technique at the HI $\gamma$ S facility, to complement unpolarized photon bremsstrahlung scattering [14]. The results of these measurements offer both an enhanced sensitivity scan of the nuclear dipole response and an unambiguous determination of spins, parities and the ground-state transition strength, which represents the elastic strength. This elastic strength governs the total photoabsorption strength from 0 MeV up to excitation energies of 2 to 3 MeV below the neutron separation energy. At excitation energies close to the neutron separation energy a significant unresolved (inelastic) strength, originating from the lower-lying excited states, is also directly measured. This strength is accumulated from either branchings of the resonance states to the low-lying states and/or resonance excitation of  $1^-$  dipole states which prefer to decay to the low-lying excited states rather than to the ground state itself.

The recent HI $\gamma$ S experiment confirmed that the branchings of the resonantly excited states are on the level of few percent [4, 8, 15], thus the inelastic strength is dominated by the inelastic transitions from the tail of the GDR. The narrow width of the beam profile at the HI $\gamma$ S facility (200–300 keV per incident energy) removed any ambiguity that these low-lying excited states can be populated from off-energy photons. Hence, NRF combined with truly monoenergetic photon beams provides direct measurements of the photoabsorption cross section below the neutron separation energy, which is a direct measure of the  $\gamma$ SF needed for inverted  $(n, \gamma)$  calculations [16].

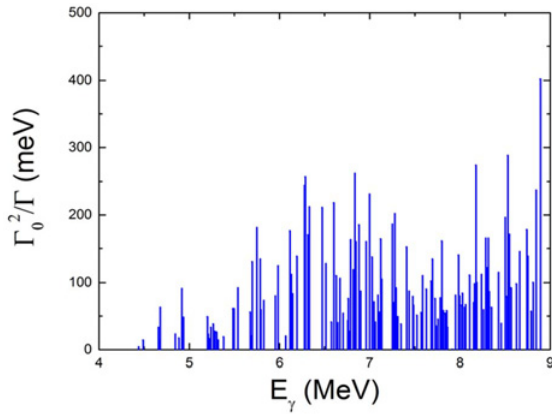


**Figure 3.**  $B(E1)\uparrow$  strength distribution for resonantly excited states in  $^{76}\text{Ge}$  between 4 and 9 MeV.

#### 4. Results

We compare the recent experimental data from two leading experimental techniques to obtain neutron capture cross sections on radioactive nuclei. We concentrated on the radioactive  $^{75}\text{Ge}$  ( $T_{1/2} = 73$  min), where a direct neutron capture cross-section measurement is not feasible. Our technique utilizes the NRF, described above, to measure the nuclear dipole response in the stable  $^{76}\text{Ge}$  [14]. The distribution of the electric dipole excited states in  $^{76}\text{Ge}$  for the energy range from 4 to 9 MeV is shown in Fig. 3. An increased density of  $1^-$  states, beginning at approximately 6.5 MeV, is apparent.

The second experimental technique utilizes the so-called Oslo methods combined with  $\beta$ -decay and  $\gamma$ -ray total absorption measurements to constrain the  $^{75}\text{Ge}(n,\gamma)^{76}\text{Ge}$  cross section [10]. This technique provides an experimental determination of the nuclear level density and  $\gamma$ -ray strength function in  $^{76}\text{Ge}$  that can be used as an input parameter for  $^{75}\text{Ge}$  capture cross-section calculation. This novel technique might open new opportunities for studying the very-rich nuclei involved in the r-process [11]. A schematic illustration of the two approaches is shown in Fig. 4. These two very different experiments, using very different data-analysis techniques, allow to obtain the  $\gamma$ SF of the same  $^{76}\text{Ge}$  compound nucleus that has been produced via  $\beta$ -decay of  $^{76}\text{Ga}$  or photon scattering of  $^{76}\text{Ge}$ . In addition, since the NRF technique is well established [4–8], it can be used to provide a benchmark for the  $\beta$ -Oslo method [10].

The nuclear dipole response in  $^{76}\text{Ge}$ , measured at the HI $\gamma$ S facility and TU Darmstadt, Germany, was used to obtain the total photoabsorption cross section below the neutron separation energy ( $S_n = 9.4$  MeV) [14]. This photoabsorption cross section was converted to  $\gamma$ SF and was directly compared with the  $\gamma$ -strength function of  $^{76}\text{Ge}$  obtained from the  $\beta$ -Oslo method [10]. Any difference between the two quantities will most likely result in different capture cross-section results of  $^{75}\text{Ge}$ . Differences between the two measurements will help to define the uncertainties of the predicted capture cross section of  $^{75}\text{Ge}$ . Reasonable agreement of the overall behavior of the  $^{76}\text{Ge}$   $\gamma$ SF is obtained from the NRF and  $\beta$ -Oslo methods (see Fig. 5).

However, there are two noteworthy differences between the measured  $\gamma$ SF from NRF and the  $\beta$ -Oslo

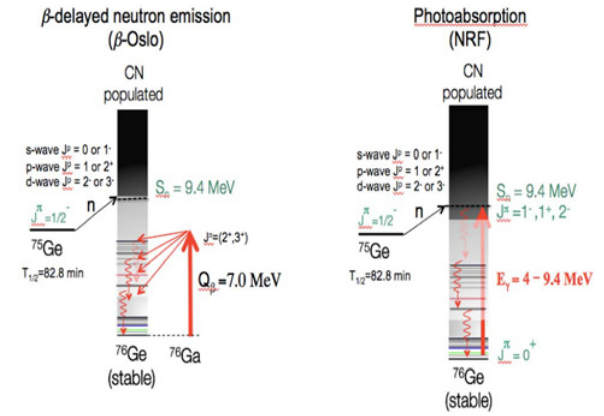


**Figure 4.** Schematic representation of the  $^{76}\text{Ge}$  production via  $\beta$ -delayed neutron emission (left panel) and photon scattering using NRF technique (right panel).

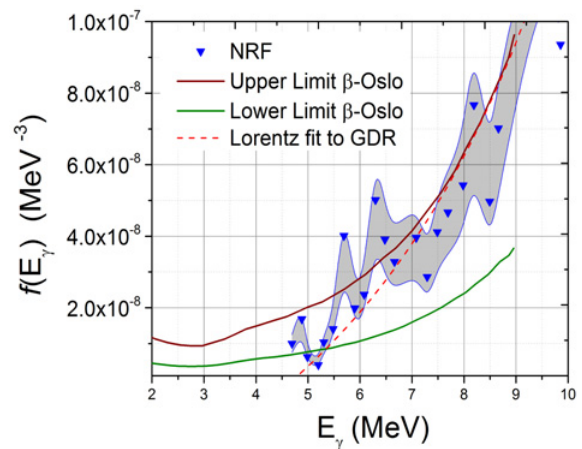


**Figure 5.**  $\gamma$ SF ( $f(E_\gamma)$ ) of  $^{76}\text{Ge}$  deduced by the NRF and  $\beta$ -Oslo methods are shown on the right panel. The gray, filled area indicates the constraints obtained with the photonscattering (NRF) data [14], while the upper and lower lines indicate the  $\gamma$ -ray strength-function limits obtained by the  $\beta$ -Oslo method [10]. The red dashed curve is the standard Lorentzian fit to the GDR, dominated by  $(\gamma, xn)$  reactions [17].

methods as shown in Fig. 5: First, the  $\gamma$ -ray strength function of  $^{76}\text{Ge}$  measured by the  $\beta$ -Oslo methods is slightly lower between 5.5–6.5 MeV, compared to the photonscattering or NRF experiment. That will reflect on slightly lower capture cross section on  $^{75}\text{Ge}$  nucleus. Second, the  $\gamma$ SF obtained by NRF technique shows more structural effects compared to the one obtained via the  $\beta$ -Oslo methods. This is most likely because of the strong individual resonances, which govern the nuclear dipole response below the neutron separation threshold of  $^{76}\text{Ge}$ .

Figure 6 displays a comparison of the neutron capture cross-section data on  $^{75}\text{Ge}$  derived from the two indirect techniques, NRF and  $\beta$ -Oslo methods. Both cross sections were obtained using the TALYS statistical code [18].

#### 5. Uncertainties implementation

Two types of uncertainties define the capture cross-section estimation. First, the experimental uncertainty (statistical and systematic) persists in any experiment. For the most of the present experiments these statistical uncertainties are easy to handle and keep under few

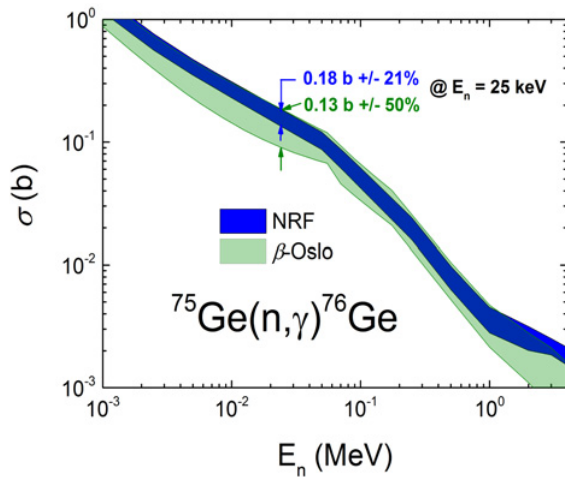


**Figure 6.** Capture cross section of the  $^{75}\text{Ge}(n,\gamma)^{76}\text{Ge}$  reaction calculated with TALYS using NRF and  $\beta$ -Oslo methods. The uncertainty band from the NRF method is due to experimental uncertainties of the  $\gamma$ SF as well as the model parameters varied in TALYS calculations.

percent or low. Systematic uncertainties are the most difficult to handle, due to some time unknown information. Second, nuclear-reaction calculations (like HF theory) use various models to describe different aspects of the reaction mechanism. This is the case in neutron capture of  $^{75}\text{Ge}$  where no direct experimental information is available. Then uncertainties occur not only in the model input parameters (sometimes adjusted to experimental data), but also in the models themselves. Another type of uncertainty comes from nuclear data evaluation. When not available experimentally, this information has to be derived from nuclear models. To investigate the impact on the model calculation capture cross-section calculations were performed with the code TALYS. We vary the most important parameters in the capture cross-section calculations such as level density models, level-density and spin cutoff parameters, the number of discrete levels, and some corresponding branching-ratio assumptions, and default optical-model potentials (local and global parameterizations). In all these cases we fix the  $\gamma$ SF and its uncertainty to the experimentally measured values and their uncertainties [14].

To assess the impact of the level density on a neutron capture cross-section calculations, we have used three phenomenological models in TALYS: the constant temperature model (CTM), the back-shifted Fermi gas model (BSFGM), and the generalized superfluid model (GM). These simple models take into account the shell, pairing and deformation effects via adjustable parameters. The goal is to match the low-energy part of the discrete levels when the  $\gamma$ SF is fixed from the experimental data [14]. The results of these calculations are shown in Fig. 7. As can be seen the difference vary between 10% at low incident neutron energies ( $E_n < 0.025$  MeV) up to 20% at higher energies ( $E_n$  around 1 MeV).

To estimate the uncertainty in the TALYS calculations originating from using a limited number of initial states with known spin and parity, two sets of identical calculations were performed [21]. In the first set of calculations, the truncation on  $J^\pi$  was set by the total amount of experimental data; i.e., all of the 111 nuclear

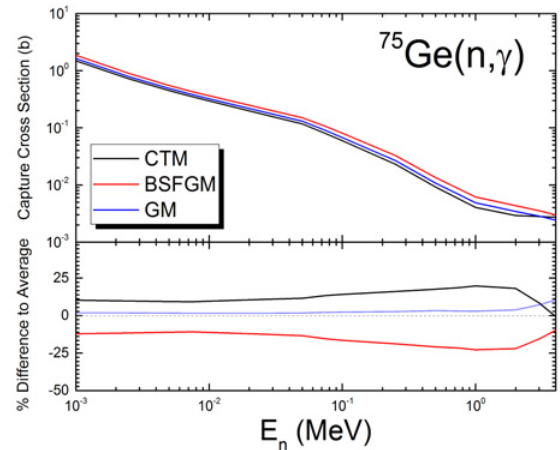


**Figure 7.** Capture cross section of  $^{75}\text{Ge}$  using three level density models (LDM) implemented in TALYS code: CTM is the constant temperature + Fermi gas model, BSFGM is the back-shifted Fermi gas model, and GM is the generalized superfluid model.

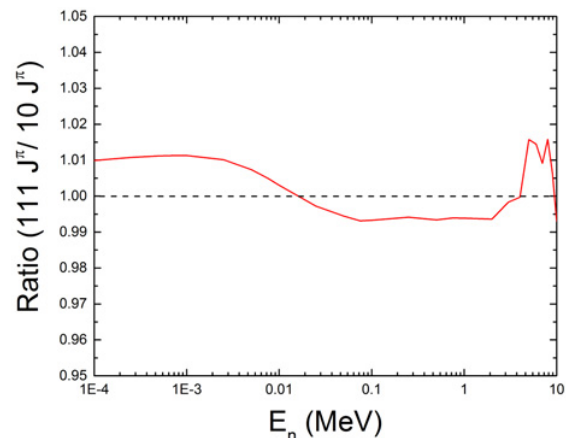


**Figure 8.** Ratio of neutron capture on  $^{75}\text{Ge}$  calculated by TALYS using complete (all known 111 levels from [20]) versus truncated  $J^\pi$  data (the first 10 known spin and parity states in  $^{76}\text{Ge}$ ).

states in  $^{76}\text{Ge}$  spanning up to 6.0 MeV. In the second set of calculations, the  $J^\pi$  data was truncated at 10 levels, which is the default value of TALYS. The results from these two sets of calculations are shown in Fig. 8.

The  $^{75}\text{Ge}(n,\gamma)$  cross section obtained this way is given in Fig. 6, with the  $\beta$ -Oslo results taken from Ref. [10]. The experimentally-constrained Maxwellian-averaged cross section at 25 keV is estimated to  $0.18 \pm 0.04$  b, a value close to KADoNis database of  $0.179 \pm 0.045$  b [19] and to the experimental value of  $0.13 \pm 0.07$  b from Ref. [10].

## 6. Conclusions

Knowing the level density and  $\gamma$ -ray strength function is mandatory to predict the capture cross section and abundances of heavy elements using astrophysical models. We demonstrated that the low-energy nuclear structure, including the PDR, plays an important role in capture cross-section calculations. The PDR lies in the region of the low-energy tail of the GDR - that is, in the broad region around the nucleon-separation energy [22].

Although the PDR exhausts only 1 to 2% of the Thomas-Reiche-Kuhn sum rule, its role in radiative processes is substantial. We also emphasize that the characteristics of the PDR in nuclei with low neutron separation energy (below 3–4 MeV) are strongly different and, consequently, phenomenological systematics based on data obtained for stable nuclei with a normal separation energy near 8 MeV might be inappropriate. In this sense, the phenomenological description is not predictive. For this reason, self-consistent microscopic approaches are needed, especially for deformed and transitional nuclei far from the line of beta-stability.

Spectroscopy information about unstable and neutron-rich nuclei, for which a direct measurements of experimental data is either impossible or very difficult, will be in ever greater demand. Fast development of techniques for physics experiments, including the advent of accelerators for studying radioactive nuclei, provides an enormous amount of experimental information, which has already been in use in nuclear data theory. Radioactive beams are now available at Argonne National Laboratory and in development at the Facility for Rare Isotope Beams, which is under construction at MSU, GANIL at France, GSI at Germany, and RIBF at Japan to provide more intense beams of isotopes far from stability. The availability of these exotic beams will make it possible to produce important isotopes using inelastic scattering and transfer reactions in inverse kinematics, as well as via  $\beta$ -decay, and to study the subsequent competition between neutron and  $\gamma$ -ray emission. Combined nuclear theory-experiment effort will be a stepping stone for a reliable, data-guided theory to gain access to capture cross section on radioactive nuclei away from the line of stability.

This work was performed under the auspices of the U.S. Department of Energy (DOE) by Lawrence Livermore National

Laboratory under contract DE-AC52-07NA27344, with partial support through LLNL's LDRD program (15-ERD-069 and 16-ERD-022).

## References

- [1] W. Hauser & H. Feshbach, *Phys. Rev.* **87**, 366 (1952)
- [2] S.P. Kamerdzhev et al., *Phys. At. Nucl.* **77**, 1303 (2014)
- [3] N. Pietralla et al., *Phys. Rev. Lett.* **88**, 012502 (2001)
- [4] A.P. Tonchev et al., *Phys. Rev. Lett.* **104**, 072501 (2010)
- [5] G. Rusev et al., *Phys. Rev. Lett.* **110**, 022503 (2013)
- [6] R. Raut et al., *Phys. Rev. Lett.* **111**, 112501 (2013)
- [7] P.M. Goddard et al., *Phys. Rev. C* **88**, 064308 (2013)
- [8] R. Schwengner et al., *Phys. Rev. C* **87**, 024306 (2013)
- [9] S. Goriely et al., *PRC* **94**, 044306 (2016)
- [10] A. Spyrou et al., *Phys. Rev. Lett.* **113**, 232502 (2014)
- [11] J.L. Tain et al., *Phys. Rev. Lett.* **115**, 062502 (2015)
- [12] J.E. Escher et al., *Rev. Mod. Phys.* **84**, 353 (2012)
- [13] J.E. Escher et al., *EPJ Web of Conferences* **122**, 12001 (2016)
- [14] R.S. Ilieva et al., submitted for publication
- [15] B. Löher et al., *Phys. Lett. B* **756**, 72 (2016)
- [16] N. Tsoneva et al., *Phys. Rev. C* **91**, 044318 (2015)
- [17] P. Carlos et al., *Nucl. Phys. A* **258**, 365 (1976)
- [18] A.J. Koning, S. Hilaire, and M. Duijvestijn, *International Conference on Nuclear Data for Science and Technology*, EDP Sciences, Les Ulis, France, 2008, p. 211
- [19] I. Dillmann et al., *Nucl. Data Sheets* **120**, 171 (2014)
- [20] National Nuclear Data Center, Brookhaven National Laboratory, USA
- [21] M. Beard, et al., *Phys. Rev. C* **90**, 034619 (2014)
- [22] D. Savran, T. Aumann, and A. Zilges, *Progress in Particle and Nuclear Physics* **70**, 210 (2013)